Supporting Information

Moxley et al. 10.1073/pnas.0811091106

SI Discussion: Metabolite-Enzyme Interaction Density in Aromatics, Arginine, and Lysine Pathways

The model illustrates that flux control (i.e., invariance to perturbation) increases as metabolite—enzyme interaction density increases. In other words, greater interaction density lessens transcriptional control and gives metabolites an increasing role in regulating the flux phenotype. This model supports the body of literature on feedback inhibition in that increased metabolite regulation of enzyme activity results in greater metabolic control. Specific biosynthesis pathways in the expanded network model provide illustrative foils for this principle (Fig. 3). Aromatics biosynthesis comprises 10 feedback inhibition and 3 feedforward activation interactions among 14 aromatic enzymes involving various pathway metabolites (Figs. 3*A* and 4*A*). Even though most mRNA and end product metabolite levels increase, high metabolite interaction density ($d_{\text{interaction}} = 13/14$) results in unchanged fluxes. This is visualized by up-regulated (green) enzyme and end product metabolite nodes and unchanging (white) flux nodes (Fig. 3*A*). The isoleucine-leucine-valine superpathway, $d_{\text{interaction}} = 7/11$ (Fig. 3*B*) corroborates this hypothesis. Despite 7 biosynthetic mRNAs increasing significantly (genewise False Discovery Rate (FDR) $< 2\%$), pathway fluxes remain unchanged (within the 3% deviation noise region). For the high metabolite interaction densities in Fig. 3 *A* and *B*, we hypothesize that because end products are not being increasingly used in protein synthesis, the metabolite levels build up and cause feedback inhibition at the enzyme level, resulting in tightly regulated flux.

In contrast, the metabolic control structures for arginine and lysine are not governed by high metabolite interaction densities (Fig. 3 *C* and *D* and 4*A*). Having only 1 of 10 enzymes regulated by enzyme-metabolite feedback inhibition (Arg-5,6p) ($d_{\text{interaction}} = 1/10$), the arginine biosynthetic pathway conforms to the null hypothesis model motivated by the central dogma. That is, activations propagate from mRNA to flux (30% deviation) to end-product metabolites, as shown by the green nodes in Fig. 3*C*. Like arginine, the lysine pathway flux, $d_{\text{interaction}} = 2/7$, increases markedly (here, 7% deviation) as a result of increasing mRNA levels, indicating less tightness in flux control (Fig. 3*D*, although the log scale does not color the flux node perceptibly green). Instead of high metabolite interaction density, arginine and lysine biosynthetic controls use alternative strategies. To compensate for unnecessary metabolite build-up, these pathways rely on preferential vacuolar localization of products and activation of transcription factor regulators separate from Gcn4p. These include the ArgR-Mcm1 repressor complex in the case of arginine and coinducers Lys14p and α-aminoadipate semialdehyde (AASA) in the case of lysine.

SI Materials and Methods

Strains. Strains were derived from the haploid S288C MAT A obtained from Dr. Gerald Fink (Whitehead Institute, Cambridge, MA). The *gcn4*Δ-knockout strain was constructed through transformation of the Saccharomyces Gene Deletion Project BY4741 gcn4Δ-knockout strain deletion cassette. This BY4741 knockout strain was obtained from the laboratory of T. Ideker (University of California San Diego, La Jolla, CA), in turn obtained through Research Genetics. Knockout strains for follow-up shake flask experimentation were constructed analogously.

Shake flask growth conditions. Strains were cultivated aerobically in 100 mL of YNB media (described above) in 500-mL shake flasks. For the met28Δ- and cbf1Δ-knockout strains, the YNB media was supplemented with 20 mg/L methionine to correct for the methionine auxotrophy. Overnight preinnoculation cultures were used to inoculate to 0.01 OD600 and grown at 30 °C until harvest at a 1.0 OD600.

Whole genome expression analysis. Our MIAME-compliant National Center for Biotechnology Information GEO submission GSE 4709 describes all experimental and data analysis considerations used for the determination of mRNA levels for the Gcn4p experiment. P-values were calculated with a Student's *t* test evaluating the wild-type and mutant mRNA levels measured in triplicate. To simultaneously test multiple hypotheses while controlling for false positives, False Discovery Rate (FDR) analysis and q-values were determined according to Storey et al. (4). For the shake flask follow-up experiments, the MIAME-compliant National Center for Biotechnology Information GEO submission GSE 7369 describes all experimental and data analysis considerations.

Biomass amino acid composition analysis. The cellular amino acid composition was determined by using ion exchange chromatography after treatment of the cell samples with 6M HCl (5). This was performed at the Center for Advanced Food Research, BioCentrum-DTU, for which they are gratefully acknowledged.

Endometabolome analysis. Cells were rapidly quenched according to de Koning and van Dam (6) in 60% (vol/vol) buffered (12.5 mM Tricine, pH 7.4) cold methanol at −40 to −45 °C. After quenching, the cells were immediately centrifuged at 10,000 × *g* for 4 min in a rotor precooled to −20 °C to separate the cells from the quenching solution. Chloroform: methanol: buffer (CMB) extraction was carried out (7). After extraction, samples were freeze-dried at low temperature (−56 °C) using a Christ-Alpha 1–4 freeze dryer (6). Amino and non-amino organic acid levels were determined by high pressure liquid chromatography on an Aminex HPX-87H column (Bio-Rad) according to Westergaard et al. (8) and by GC-MS analysis according to Villas-Boas et al. (9) except that a Finnegan FOCUS gas chromatograph coupled to single quadrupole mass selective detector (EI) (Thermo Electron) was used. Peak enumeration was conducted with AMDIS (NIST) with default parameters, and identification of conserved metabolites was conducted with SpectConnect (10) using default parameters and a support threshold of 3.

Exometabolome analysis. Culture samples for determination of exometabolites were immediately filtered through a 0.22-mm-pore-size cellulose acetate filter (CAMEO 25GAS 0.22, Osmonics, Minnetonka, MN, USA) according to Westergaard et al. (8). GCMS and HPLC analysis was performed as indicated above.

1. Antoniewicz MR, Kelleher JK, Stephanopoulos G (2006) Determination of confidence intervals of metabolic fluxes estimated from stable isotope measurements. *Metab Eng* 8:324–337.

2. Antoniewicz MR, Kelleher JK, Stephanopoulos G (2007) Elementary metabolite units (EMU): A novel framework for modeling isotopic distributions. *Metab Eng* 9:68–86.

3. Antoniewicz MR, et al. (2007) Metabolic flux analysis in a nonstationary system: fed-batch fermentation of a high yielding strain of E. coli producing 1,3-propanediol. *Metab Eng* 9(3):227–292.
4. Storey JD, Tibshirani R (2003) Statistical significance for genomewide studies. *Proc Natl Acad Sci USA* 100:9440–9445.
5. Barkholt V, Jensen AL (1989) Amino acid analysis: determination of cysteine plus half-cystine in proteins after hydrochloric acid hydrolysis with a disulfide compound as additive. *Anal Biochem* 177:318–322.
6. de Koning W, van Dam K (1992) A method for the determination of changes of glycolytic metabolites in yeast on a subsecond time scale using extraction at neutral pH. *Anal Biochem* 204:118–123.
7. Villas-Boas SG, Hojer-Pedersen J, Akesson M, Smedsgaard J, Nielsen J (2005) Global metabolite analysis of yeast: evaluation of sample preparation methods. *Yeast* 22:1155–1169.
8. Westergaard SL, Oliveira AP, Bro C, Olsson L, Nielsen J (2006) A systems biology approach to study glucose repression in the yeast Saccharomyces cerevisiae. *Biotechnol Bioeng* 96:134–145.
9. Villas-Boas SG, Moxley JF, Akesson M, Stephanopoulos G, Nielsen J (2005) High-throughput metabolic state analysis: the missing link in integrated functional genomics of yeasts. *Biochem J* 388(Pt 2):669–677.
10. Styczynski MP, et al. (2007) Systematic identification of conserved metabolites in GC/MS data for metabolomics and biomarker discovery. *Anal Chem* 79(3):966–973.

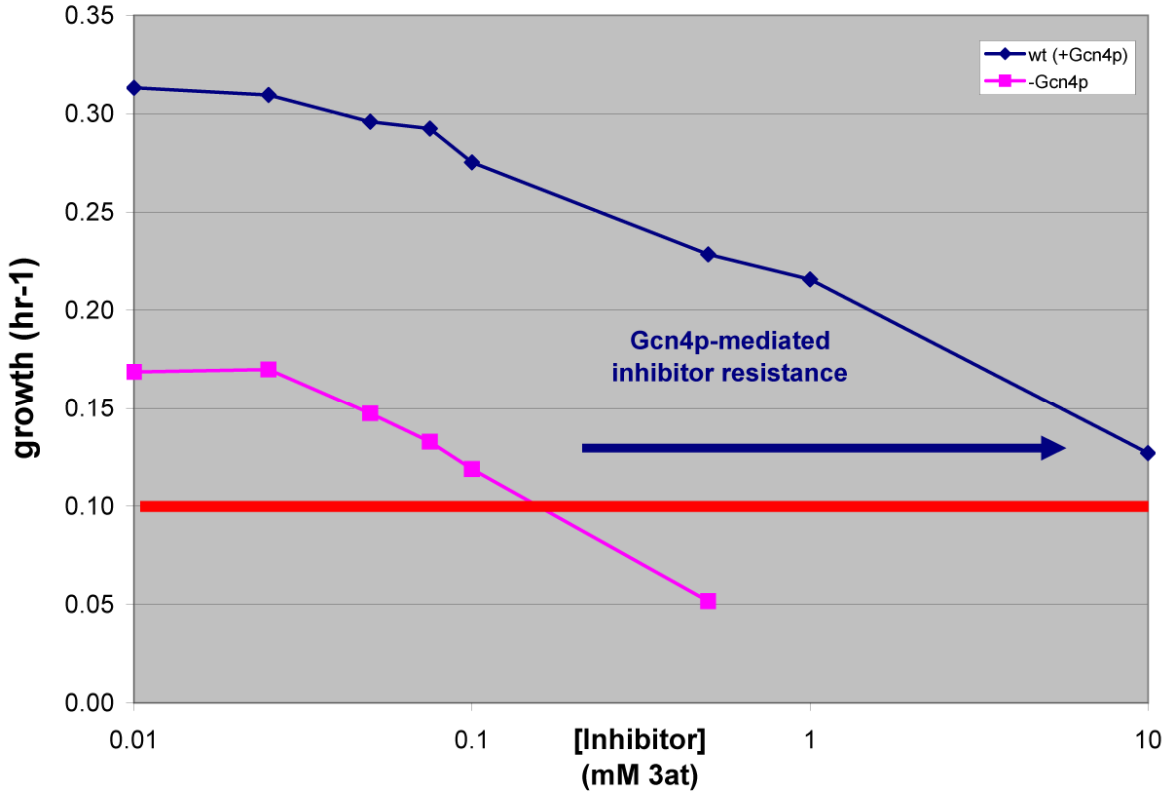

Fig. S1. Gcn4p-mediated induction of histidine biosynthetic mRNAs conferred ≈100-fold increased resistance to 3AT. Wild-type yeast and a *gcn4*Δ-knockout strain (i.e., response present versus absent) were cultivated in triplicate at varying concentrations of histidine biosynthetic inhibitor 3AT. Growth curves were measured with a Bioscreen C (Growth Curves) and growth constants determined at early log phase. For chemostat operation at a dilution of 0.10 h^{-1} (depicted in the red line), inhibitor levels of 10 mM for the wild type and 0.1 mM for the *gcn4*Δ strain create a near starvation state for histidine. We note that the ≈100-fold increase in inhibitor resistance at dilutions of 0.10 h^{-1} are mediated by Gcn4p activation of biosynthetic enzymes.

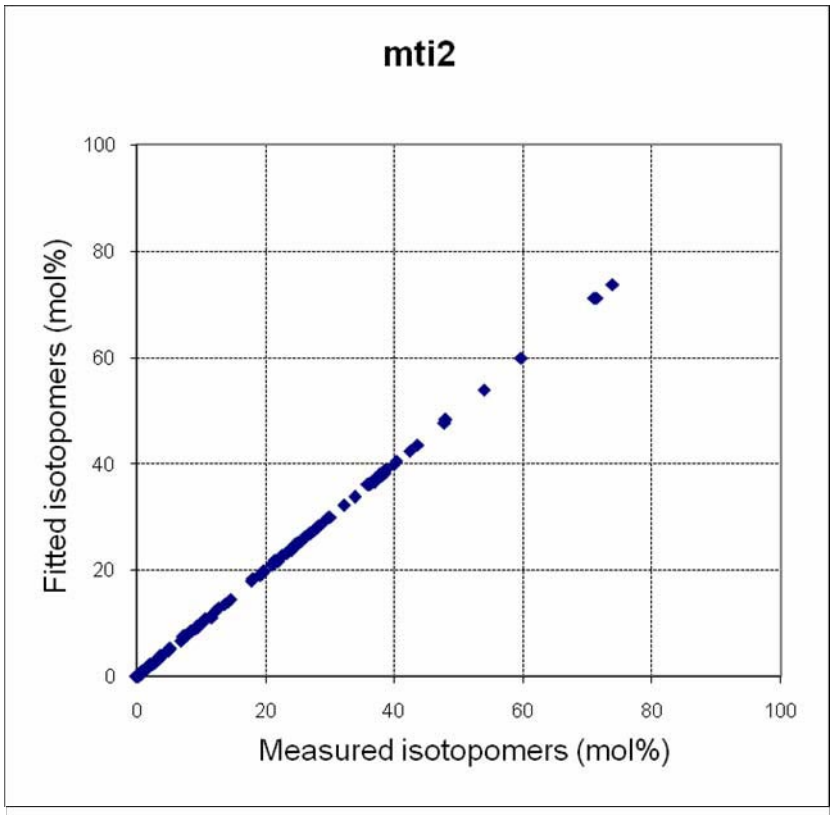

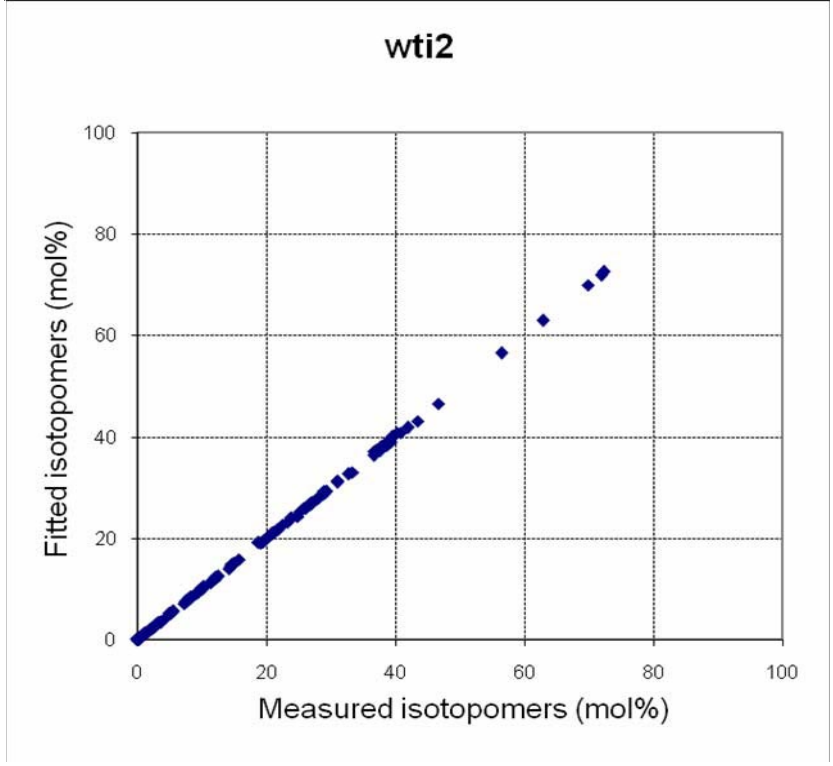

Fig. S2. Comparisons of mass isotopomer distributions of biomass amino acids between fitted values and values measured by GC-MS reveal an excellent quality of fit. For this reason, we have a high degree of confidence in our experimentally-determined fluxes. (*Upper*) Data from the chemostat without Gcn4p-mediated induction. (*Lower*) Data from the chemostat with Gcn4p-mediated induction.

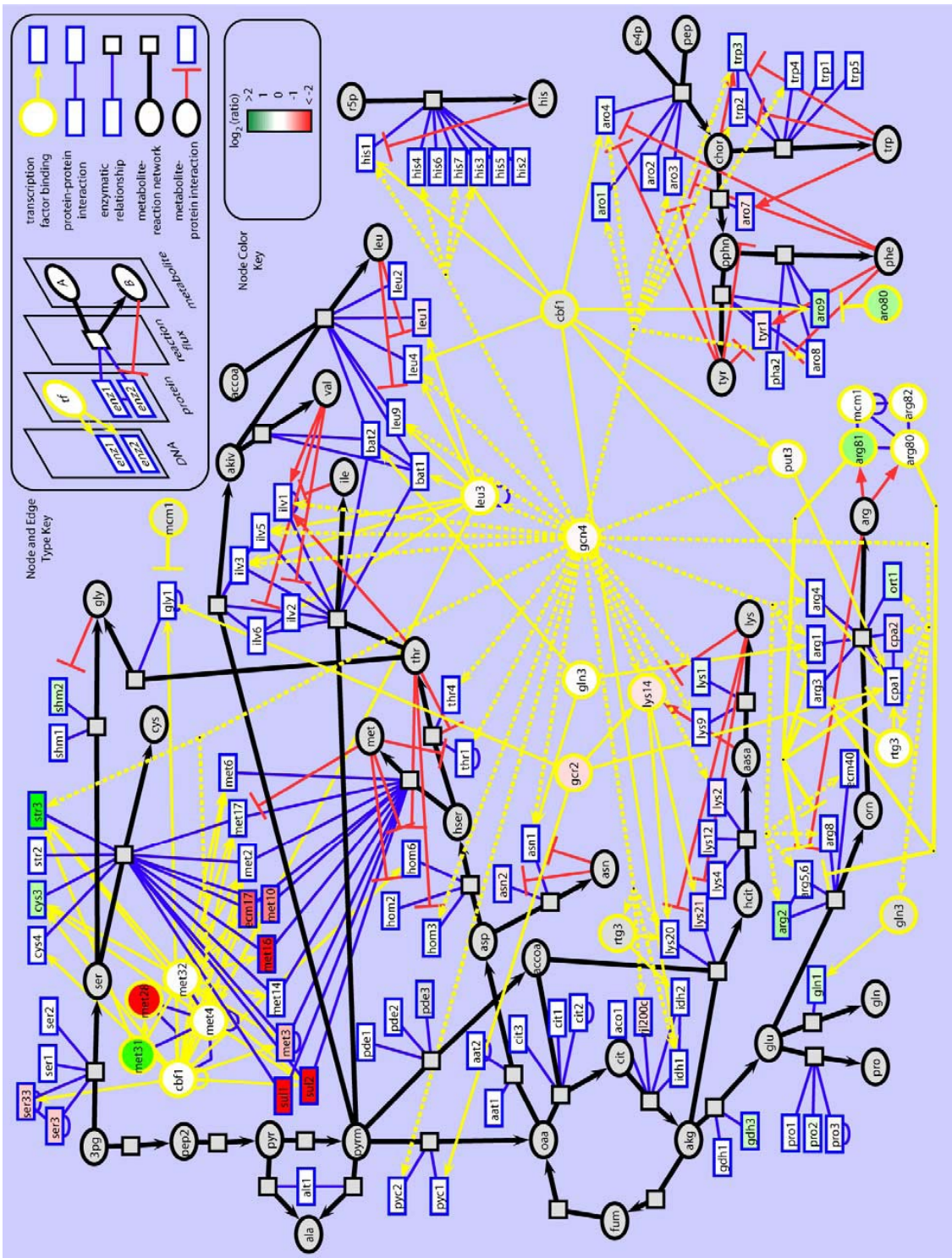

Fig. S3. mRNA levels for the *met28*Δ mutant relative to the wild type visualized on our model of amino acid biosynthesis. See Fig. 3 for further description of the model and visualization.

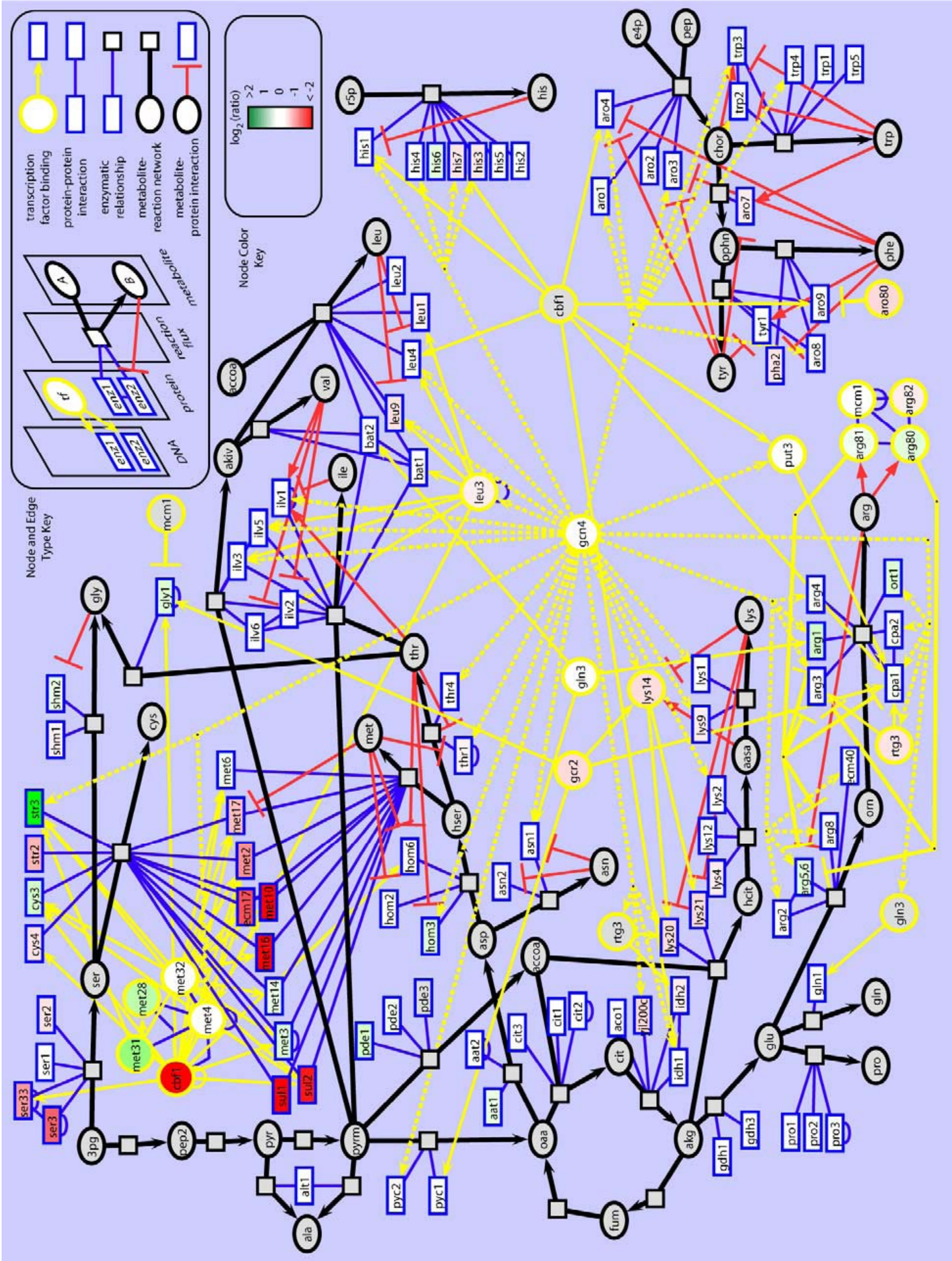

Fig. S4. mRNA levels for the *cbf1*Δ mutant relative to the wild type visualized on our model of amino acid biosynthesis. See Fig. 3 for further description of the model and visualization.

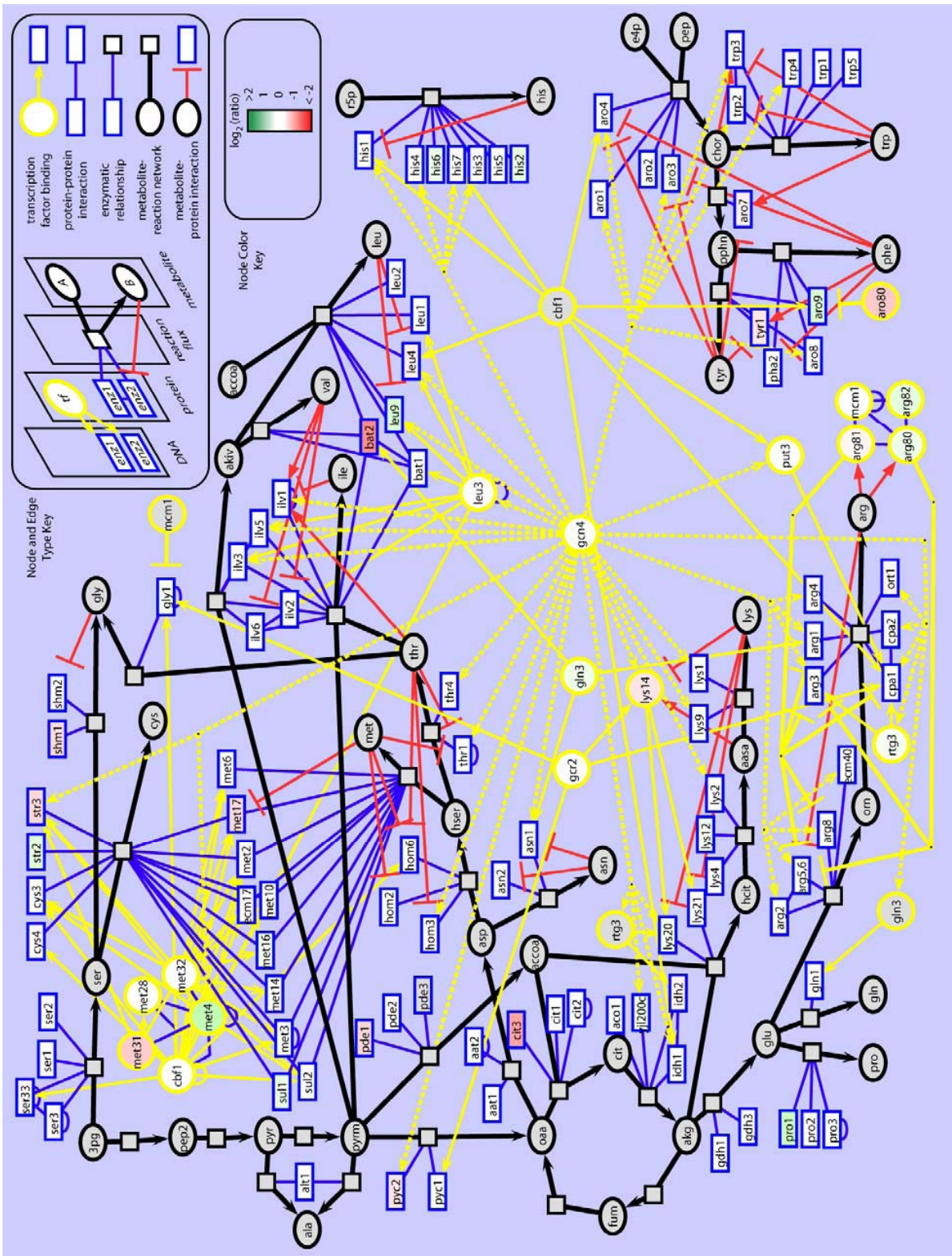

Fig. S5. mRNA levels for the *met31*Δ mutant relative to the wild type visualized on our model of amino acid biosynthesis. See Fig. 3 for further description of the model and visualization.

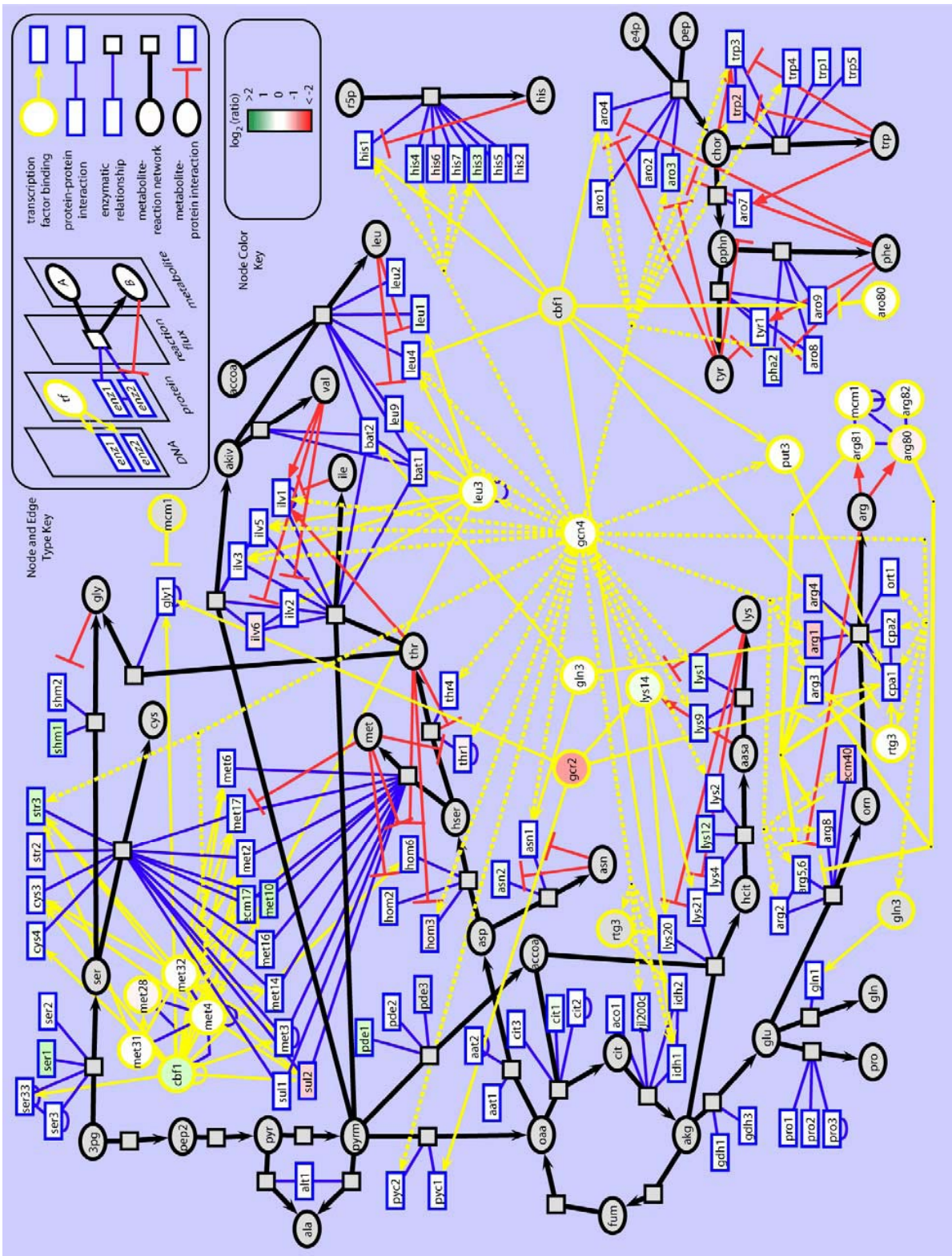

Fig. S6. mRNA levels for the *met32*Δ mutant relative to the wild type visualized on our model of amino acid biosynthesis. See Fig. 3 for further description of the model and visualization.

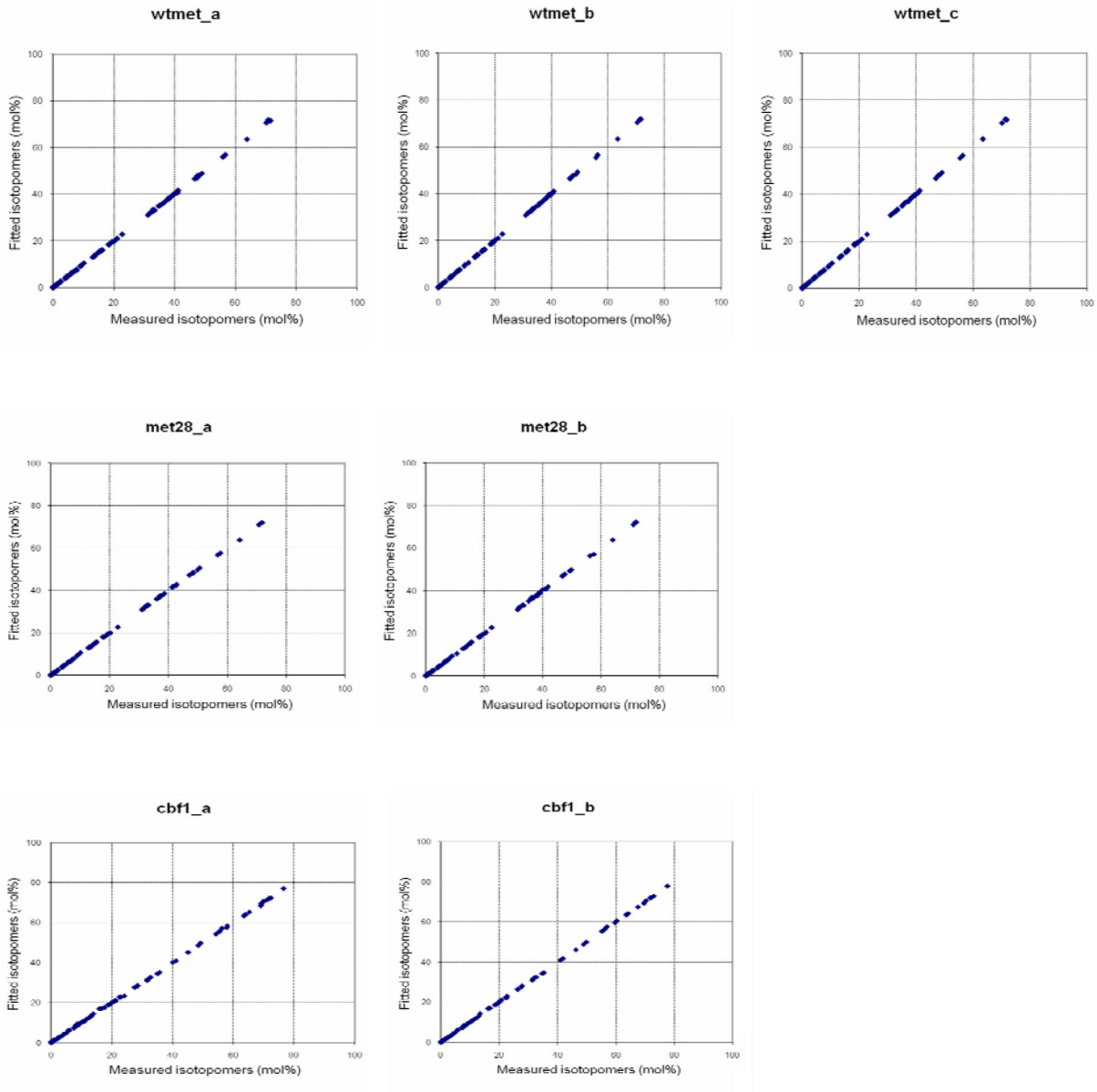

Fig. S7. Comparisons of mass isotopomer distributions of biomass amino acids between fitted values and values measured by GC-MS reveal an excellent quality of fit. For this reason, we have a high degree of confidence in our experimentally-determined fluxes. (*Top*) Data from 3 wild-type shake flasks. (*Middle*) Data from *met28*Δ mutant shake flasks. (*Bottom*) Data from the *cbf1*Δ mutant.

Table S1. New observations and hypothetical biological principles

	Observations	Biological principles
1	Despite fermenting at macroscopically-equivalent steady states, expression levels of genes in amino acid biosynthesis are, in general, activated relative to *gcn4*Δ populations (Fig. 3)	To compensate and counteract for broad transcriptional changes, cells use metabolic control mechanisms
2	Changes in flux do not correlate with changes in mRNA levels along the pathway (Fig. 2B)	Greater metabolite interaction densities can give pathways greater flux invariance to perturbation
3	Changes in metabolite levels do not correlate with changes in mRNA levels along the pathway (Fig. 2C)	Metabolite levels are a complex function of mRNA levels, enzyme activities, metabolite interaction strengths, kinetics, spatial distributions, and upstream and downstream supply and demand.
4	Changes in metabolite levels do not correlate with changes in flux along the pathway (Fig. 2D)	In some instances, greater densities and strengths of metabolite interactions allow buildup of metabolites without significant flux changes
5	Metabolic flux is rewired in metabolic networks in the presence of altered transcriptional states (Fig. 3)	Transcriptional regulatory networks drive not only mRNA changes but propogate rewiring of flux through the metabolic network as a mechanism for physiological stress response

Table S2. New observations, example hypotheses, and possible tests

	Specific systems-level observations[†]	Hypothesis	Test
1	Aromatic biosynthesis: 12 of 14 mRNAs increase significantly (FDR $<$ 2%), fluxes remain unchanged (less than 3% deviation), and phenylalanine and tyrosine levels rise 4-fold and 8-fold, respectively (Fig. 3A)	Higher density of metabolite-enzyme interactions affords increased flux control (invariance during perturbation)	Examine flux and metabolite profiles in a strain with mutated feedback inhibition regions in *ARO4, ARO3, TRP2, TRP3, PHA2,* and *TYR1*[‡]
2	Isoleucine-leucine-valine biosynthesis: 7 of 11 mRNAs increase significantly (FDR $<$ 2%), pathway fluxes remain unchanged (less than 3% deviation), isoleucine, valine, and leucine levels increase approximately 2-fold (Fig. 3B)	Higher density of metabolite-enzyme interactions affords increased flux control (invariance during perturbation)	Examine flux and metabolite profiles in a strain with mutated feedback inhibition regions in *ILV1, ILV2, ILV6, LEU4,* and *LEU9*[‡]
3	Arginine biosynthesis: excluding *CPA1*, mRNAs increase significantly ($P < 0.002$), flux increases (30% $>$ 3%), and arginine level increases 8-fold (Fig. 3C)	Arginine levels are primarily regulated downstream of arginine biosynthesis	Examine gene expression, flux, and metabolite profiles in a strain lacking arginine catabolic enzymes and/or having limited vacuolization capabilities[‡]
4	Lysine biosynthesis: 5 of 7 mRNAs increase significantly (FDR $<$ 2%), flux significantly increases (7% $>$ 3% deviation), lysine level increases 4-fold (Fig. 3D)	Lysine levels are primarily regulated downstream of lysine biosynthesis	Examine gene expression, flux, and metabolite profiles in a strain with mutated binding sites for the transcriptional activator *LYS14* and/or having limited vacuolization capabilities[‡]
5	Aspartate, threonine and glycine biosynthesis: 6 of 8 mRNAs increase significantly (FDR $<$ 2%), flux shifts from serine to the threonine precursor, threonine and aspartate levels do not change, glycine levels decrease 4-fold (Fig. 3E)	Transcriptional activation rewires glycine flux through the aspartate and threonine nodes	Examine growth rate in a mutant lacking glycine biosynthesis from serine at increasing levels of threonine supplementation[‡]
6	Alanine biosynthesis: mRNA level increases significantly (FDR $<$ 2%), flux shifts from the mitochondria to the cytosol, alanine levels decrease 4-fold (Fig. 3)	Cytosolic pools of pyruvate are increased in the presence of Gcn4p to increase cytosolic flux by mass action kinetics	Examine cytosolic and mitochondrial pools of pyruvate in wild type and *gcn4*Δ strains[‡]
7	*SER3, SER1,* and *SER2* mRNA levels increase, but flux through the reaction they catalyze decreases (Fig. 3)	The transcriptional rewiring of glycine flux results in less flux through serine into glycine	Examine growth rate in a mutant lacking glycine biosynthesis from serine at increasing levels of threonine supplementation[‡]
8	Transcription factors Met4p, Leu3p, and Lys14p genes are bound yet not activated (Fig. 2A)	Gcn4p is a necessary but not sufficient for activation	Compare the transcriptional profile of *MET4, LEU3,* and *LYS14* in yeast strains which overexpress other known transcription factors with wild type cells[‡]
9	*CPA1* genes are bound yet not activated (Fig. 2A)	10-fold increase in free arginine levels destabilizes the mRNA in a uORF-mediated mRNA decay interaction	Observe CPA1 mRNA levels in varying levels of intracellular arginine
9	4-fold increase of unbound *ARO9* (Fig. 2A)	Increase in free phenylalanine and tyrosine levels in an observed ARO80-mediated transcriptional activation	Observe ARO9 mRNA levels in varying levels of supplemented phenylalanine and tyrosine
10	Despite an unchanged mRNA profile, Leu3p's binding targets have increased mRNA levels (Fig. 3)	Leu3p's role as a transcriptional activator is secondary to Gcn4p	Compare transcript levels of the isoleucine-leucine-valine biosynthetic pathway in wild type and *leu3* knockdown strain[‡]

[†]Given for wild type relative to gcn4Δ cell populations. Both cell populations were grown at the same rate and had the same biomass.
[‡]Performed under conditions where the Gcn4p mediated stress response has been activated

Table S3. Wild-type yeast and a gcn4Δ-knockout strain ferment at macroscopically-equivalent steady states with regard to growth rate, cell density (biomass), and ethanol and CO_2 production

	Dilution rate, h^{-1}	Biomass yield, C-moles	Glyc, g/L	Ace, g/L	Eth, g/L	CO_2, % offgas
Fermentative steady state	0.10 ± 0.01	0.17 ± 0.03	0.05 ± 0.01	0.06 ± 0.01	1.7 ± 0.2	0.32 ± 0.02

Other Supporting Information Files

Dataset S1
Dataset S2
Dataset S3
SI Appendix